Characterization of Niobia-Supported Palladium−Cobalt Catalysts

F. B. Noronha[†] and Martin Schmal*

NUCAT-PEQ-COPPE, Universidade Federal do Rio de Janeiro, Ilha do Fundão, COPPE, C.P.68502, CEP 21941, Rio de Janeiro (Brasil)

B. Moraweck, P. Delichère, and M. Brun

IRC/CNRS, 2 Av. Albert Einstein, 69626 Villeurbanne Cedex, France

F. Villain[‡]

LURE, Bâtiment 209d, Centre Universitaire Paris - Sud, BP 34, 91898 Orsay Cedex, France

R. Fréty

Laboratoire d'Application de la Chimie à l'Environnement, LACE/CNRS, 43 Bd du 11 novembre 1918, 69622 Villeurbanne Cedex, France

Received: August 5, 1999; In Final Form: February 15, 2000

Niobium oxide supported Pd−Co catalysts were characterized through XPS (X-ray photoelectron spectroscopy), (XPS), temperature-programmed reduction (TPR), magnetic measurements, X-ray diffraction, and extended X-ray absorption fine structure (EXAFS). XPS analyses suggested the presence of Co_3O_4 particles and Co^{2+} surface phase. TPR and magnetic measurements showed that the palladium addition promoted not only the reduction of Co_3O_4 particles but also the cobalt surface phase. Magnetic measurements and EXAFS analyses revealed the Pd−Co alloy formation during reduction. A model represented by bimetallic particles enriched with palladium and particles containing only cobalt was proposed.

Introduction

Monometallic cobalt catalysts are effective for the synthesis of long-chain hydrocarbons from hydrogen and carbon monoxide.[1−3] The catalytic hydrogenation (activity, selectivity, and stability) of carbon monoxide on cobalt catalysts has been reported to be affected by two factors: the dispersion and the extent of reduction.[4−7] The reducibility of cobalt is closely related to the nature of the species present on the support. In particular, on supported cobalt catalysts, several cobalt species have been detected as a function of the support.[8−13] At least three different types of cobalt species have been reported on the alumina-supported cobalt catalysts: Co_3O_4 particles, which are more readily reduced; Co^{2+} species and $CoAl_2O_4$, which are hardly reduced or unreduced, respectively.[8,14−16] On niobia-supported cobalt catalysts, X-ray photoelectron spectroscopy (XPS), diffuse reflectance spectroscopy (DRS), and temperature-programmed reduction (TPR) analysis revealed that catalysts with low cobalt content showed a high amount of Co^{2+} species in interaction with the support. For higher cobalt loading, Co_3O_4 particles were also present, in addition to Co^{2+} species.[12]

Besides the support, the addition of noble metals to a supported cobalt catalyst can also change the cobalt state and modify its activity and selectivity.[17−21] An enhancement of the activity of cobalt with the addition of small amounts of Pd[20] or Pt[21] has been reported. In general, it has been proposed that the addition of a noble metal promotes the cobalt oxide reduction.[20−27] A larger fraction of metallic cobalt could explain the catalytic behavior of these bimetallic catalysts. Moreover, adding a second metallic element can lead to alloy formation, which could change the catalytic and adsorptive properties.[28,29] For example, the addition of a noble metal to iron or cobalt catalyst increases the selectivity of synthesis gas reaction toward methanol.[17,30−33] The addition of Fe to Pd resulted in significant enhancement of methanol formation which was ascribed to Pd_xFe alloy formation. According to Guczi,[31] the nonreducible oxide-metal interface or the alloy formation induces two effects: modification of both the CO adsorption mode (CO dissociation or adsorption in a molecular form) and the adsorption of hydrogen. In both cases, the $CO + H_2$ selectivities should be altered by the bimetallic catalysts. Furthermore, the second metal component can also modify the deactivation behavior.[34]

The addition of noble metal to Co/Nb_2O_5 catalysts showed interesting selectivity results on the Fischer−Tropsch synthesis.[35] The presence of a noble metal increased the C_5^+ selectivity and decreased the methane formation independent of the reduction temperature. However, the characterization of the reduced state was not performed, making difficult a complete comprehension of the catalytic behavior.

In fact, relatively few studies have been done to investigate the behavior of bimetallic systems on a support able to promote the strong metal support interaction (SMSI) effect, such as Nb_2O_5.[36−38] This may be explained by the difficulties of the niobium oxide supported catalysts characterization. Techniques such as X-ray diffraction (XRD)[39] and energy-dispersive X-ray

[†] Present address: Instituto Nacional de Tecnologia − INT, Av. Venezuela 82, CEP 20081-310, Rio de Janeiro, Brasil.

[‡] Present address: Laboratoire de Chimie Inorganique et Matériaux Moléculaires, Case 42, Bâtiment F74, Université Pierre et Marie Curie, 4 place Jussieu, 75252, Paris Cedex 05, France.

* For correspondence. E-mail: schmal@peq.coppe.ufrj.br.

10.1021/jp992777o CCC: $19.00
Published on Web 05/19/2000

TABLE 1: Catalyst Composition (Pd_xCo_y)[a]

	composition (wt %)	
catalyst	Pd	Co
Pd/Nb_2O_5	1.3	−
$Pd_{35}Co_{65}/Nb_2O_5$	2.1	2.1
$Pd_{15}Co_{85}/Nb_2O_5$	1.6	5.0
Co/Nb_2O_5	−	2.0

[a] *x* and *y* represent the atomic percent of Pd and Co.

spectroscopy (EDS)[40] are not appropriate to detect the formation of a solid solution and to estimate alloy composition. In XRD, the problem is caused by both superposition of the line characteristics of the metal by the support and the weak metals concentrations. Conventional electron microscopy technique cannot identify the particles because of the contrast problems between the metals and the niobium oxide. Furthermore, IR spectroscopy analysis of adsorbed carbon monoxide, in the transmission mode, efficient for some bimetallic catalysts,[41] cannot be used to probe the state of the surface of niobia-supported catalysts because of the partial reduction of the support.

In this work, we studied the characterization of Pd−Co catalysts supported on niobium oxide. To overcome the difficulties presented by this system and based on our previous knowledge of the Pd−Co interaction,[42,43] we used TPR and magnetic measurements to study the formation of bimetallic particles on $Pd-Co/Nb_2O_5$ catalysts. Evidence of the alloy formation was obtained through extended X-ray absorption fine structure (EXAFS) technique. A model for these calcined precursors was also proposed based on XPS analysis and TPR results.

Experimental Section

Catalyst Preparation. The Nb_2O_5 support (Brunauer−Emmett−Teller area, 30 m^2/g) was obtained by calcination of niobic acid (CBMM, HY 340, AD929) in air at 823 K for 2 h. The catalysts were prepared by incipient wetness impregnation or coimpregnation of the support with an aqueous solution of palladium nitrate and cobalt nitrate, followed by drying at 393 K for 16 h and calcination in air at 673 K for 2 h. Table 1 lists the catalysts and their metal contents, measured by atomic absorption spectroscopy.

XPS. The XPS analyses were performed in a VG ESCALAB 200R spectrometer using monochromatic Al K_α and Mg Kα radiation. The residual pressure in the analysis chamber during the measurements was about 5×10^{-9} mbar. The Co 2p, Pd 3d, Nb 3d, O 1s, and C 1s regions were recorded using a pass energy of 50 eV. The charge of catalyst samples was corrected by setting the binding energy (BE) of Nb 3d at 207.5 eV for the niobia support.[44] Surface compositions were calculated from photoelectron peak areas after correction by the photoionization cross-sections[45] and electron escape depth.[46]

TPR. TPR measurements were performed in a flow system as described previously.[36] Before reduction, the catalysts were flushed under argon at 423 K. TPR analysis was performed by using a mixture of 1.3% hydrogen in argon (flow rate, 30 cm^3/min). The hydrogen consumption was measured as the temperature was raised at 10 K/min, up to 1173 K. The sample weight was selected to ensure ca. 0.01 g of the active phase (Pd + Co).

Magnetic Measurements. The analysis and equipment were similar to those described elsewhere.[43] The cell for magnetic measurements was coupled, on line, to a TPR apparatus, which was equipped with a thermal conductivity detector and a quadrupolar mass spectrometer. This approach allowed the measurement of the magnetic properties of cobalt at well-defined temperatures during the TPR (298, 473, and 873 K).

The catalysts were reduced under a flow mixture of 1% hydrogen in argon. At the desired temperature, the reduction was stopped by sample quick cooling, and the magnetization was measured at 298 K using the extraction method of Weiss.[47,48] Magnetic measurements gave information on both the amount of metallic cobalt and alloy formation.

XRD. X-ray diffraction patterns of the reduced catalysts were performed on a D500 Siemens goniometer (Mo Kα radiation, $\lambda = 0.71073$ Å) coupled to a high-temperature chamber.[40] This system led to patterns of the reduced samples, without exposure to air. The catalyst was previously reduced by hydrogen at 773 K. The data were recorded using a position-sensitive proportional counter Raytech in the scanning mode and processed with the Diffract-AT software (Socabim).

EXAFS. EXAFS experiments were performed after reduction of the precursors in flowing hydrogen at 773 K (1 h, 60 mL/min). Then, the samples were transferred into special sample holders under dry nitrogen and protected by a Kapton window to prevent any air contamination during the EXAFS experiments. Detection in fluorescence mode was chosen because of the large absorption of the niobia carrier at the energies of palladium (24350 eV) and cobalt (7707 eV) K edges. A copper foil (0.2 mm thick) was inserted before the detector window to avoid the saturation of the detector (Ge−Li) by the niobium fluorescence (16614 eV) at the Pd K edge. The niobium fluorescence was then eliminated by energy discrimination to keep only the photons emitted by the Pd or Co elements in the sample. The range in energy was about 1000 eV around each edge. An energy step of 4 eV (Pd) and 2 eV (Co) and a counting time of 5 s at each data point were used. The extraction of the oscillatory part of the absorption signal was performed by a standard method.[49] At first, a straight line was fitted to the preedge and extrapolated at energies higher than the edge. Then, a polynomial of 4 to 7 degrees was used to fit the atomic-like absorption coefficient and the data were normalized using the Eisenberger−Lengeler method.[50] The k^3 weighted $\chi(k)$ function was then Fourier transformed from $k = 3-13$ A^{-1} (or 15 $Å^{-1}$ in the cobalt edge) using a Kaiser window ($\tau = 9$). The peak corresponding to the first coordination sphere was then isolated and back-Fourier transformed into *k* space to determine the mean coordination number, *n*, the bond-length, *R*, and the Debye−Waller-like factor $\Delta\sigma$ by a fitting procedure using the simplex method.[51] A Pd foil (15 μm thick) and a Co foil (4 μm thick) were used to extract the backscattering amplitude and phase functions for the Pd−Pd and Co−Co pairs, respectively. For the Pd−Co and Co−Pd pairs, the results of the theoretical work by Rehr[52] were used.

The quality of the fit was determined by a reliability factor defined as[40]:

$$Q = \sum_i \frac{[k^3(|\chi_i^c(k)| - |\chi_i^e(k)|)]^2}{(k^3\chi_i^e(k))^2}$$

Results and Discussion

State of the Precursor. XPS results are presented in Table 2. For the Pd/Nb_2O_5 and $PdCo/Nb_2O_5$ samples, the Pd $3d_{5/2}$ BE were 337.0 and 336.9 eV, according to those observed for PdO.[53,54]

XPS Co 2p spectra of Co/Nb_2O_5 and $PdCo/Nb_2O_5$ catalysts are shown in Figure 1. On Co/Nb_2O_5 catalyst, the Co $2p_{3/2}$ and

TABLE 2: Experimental Binding Energies (BE) and XPS Atomic Ratios of the $PdCo/Nb_2O_5$ Catalysts

	binding energy (eV)			atomic ratio			ΔE^a
catalyst	$Pd_{3d5/2}$	$Co_{2p3/2}$	O_{1s}	Pd/Nb	Co/Nb	Pd/Co	(eV)
Pd/Nb_2O_5	337.0	–	530.5	0.007	–	–	–
$Pd_{35}Co_{65}/Nb_2O_5$	336.9	781.3	530.9	0.009	0.040	0.225	16.1
$Pd_{15}Co_{85}/Nb_2O_5$	337.0	779.8	530.5	0.016	0.204	0.078	15.6
Co/Nb_2O_5	–	781.5	530.6	–	0.140	–	15.8

[a] $\Delta(E_{Co2p1/2} - E_{Co2p3/2})$.

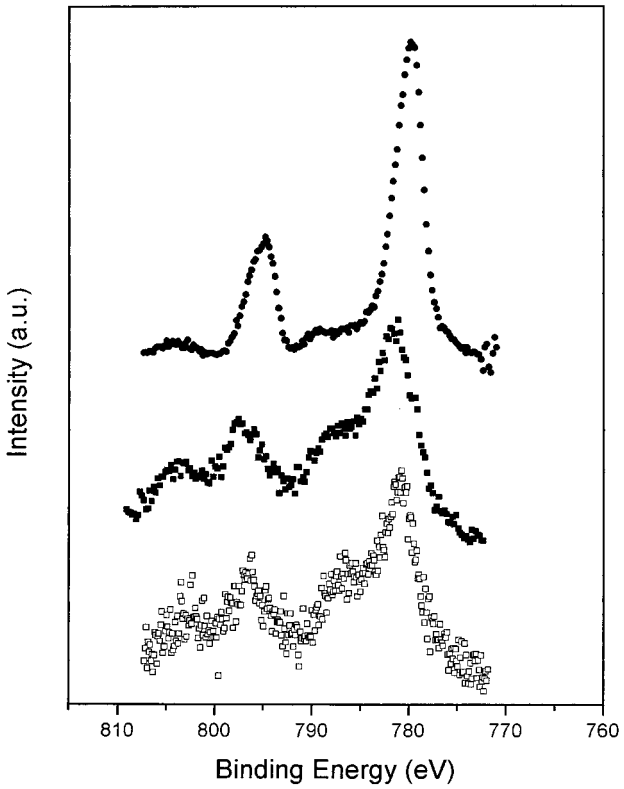

Figure 1. XPS Co 2p spectra of the calcined $Pd-Co/Nb_2O_5$ catalysts. (□) Co/Nb_2O_5; (■) $Pd_{35}Co_{65}/Nb_2O_5$; (●) $Pd_{15}Co_{85}/Nb_2O_5$.

Co $2p_{1/2}$ peaks presented BE at 781.5 and 797.4 eV, respectively ($\Delta E_{Co\ 2p1/2\ -\ Co\ 2p3/2} = 15.8$ eV). Furthermore, the intensity of the satellite peak around 786 eV was high (satellite/principal ratio = 0.38). The XPS spectrum of the $Pd_{35}Co_{65}/Nb_2O_5$ bimetallic catalyst exhibited a Co $2p_{3/2}$ peak at 781.3 eV, a strong shake-up satellite peak around 786 eV, and a spin−orbit coupling of 16.1 eV. The Co 2p spectrum of the $Pd_{15}Co_{85}/Nb_2O_5$ catalyst showed a weak satellite peak and a spin−orbit splitting of 14.9 eV. In addition, the Co $2p_{3/2}$ BE was lower than that of the catalysts with low cobalt content.

The BE, the line shapes, and the intensity of the satellite peaks have often been used for identification of the cobalt species.[8,13,14,55] The reported average BE values for bulk Co_3O_4[12−14,55−60] and CoO[12,55−59,61,62] are 779.9 and 780.4 eV, respectively. These BE values are too close and cannot be distinguished clearly.[52,55] On the other hand, the intensities of the shake-up satellites associated with the Co $2p_{3/2}$ peaks of both oxides are quite different. The satellite peak is practically absent on Co_3O_4 whereas it is very strong on CoO. In addition, the spin−orbit coupling of the CoO is approximately 1 eV higher than the one for the Co_3O_4 (Table 3). On the other hand, the intensity of the shake-up satellite and the spin−orbit coupling of cobalt niobate compound are similar to those displayed by CoO. Therefore, it is very difficult to determine through the features of the Co 2p spectra whether the Co^{2+} species are present as cobalt niobate or as CoO on the niobia supported catalysts.

TABLE 3: Hydrogen Consumption (μmol H_2/mg Metal) in the TPR Analysis

	experimental			theoretical[a]	
catalyst	T_{amb}	298−473 K	473−873 K	Pd	Co
Pd/Nb_2O_5	10.8	−1.4	1.4	9.4	–
$Pd_{35}Co_{65}/Nb_2O_5$	6.4	2.0	6.5	4.7	11.4
$Pd_{15}Co_{85}/Nb_2O_5$	4.1	4.8	12.8	2.3	17.2
Co/Nb_2O_5	–	–	18.4	–	22.6

[a] Theoretical H_2 uptake corresponds to the following reactions: Pd T_{amb}: $PdO \rightarrow Pd^\circ$ Co 298−473 K: $Co_3O_4 \rightarrow CoO$ 473−873 K: $CoO \rightarrow Co^\circ$ $Co^{2+} \rightarrow Co^\circ$

Recently, Noronha et al.[12] performed XRD, DRS, and XPS analyses on reference compounds (Co_3O_4, CoO, and two cobalt niobates calcined at 873 and 1173 K) and Co/Nb_2O_5 catalysts with different cobalt loading. The XPS spectra of the 1% and 2% Co/Nb_2O_5 catalyst showed a strong shake-up satellite and a spin−orbit coupling of 16.1 and 15.6 eV, respectively. On the other hand, the Co $2p_{3/2}$ spectra of 5% and 10% Co/Nb_2O_5 catalyst exhibited a weak satellite peak and a spin−orbit splitting of 15.2 and 15.4 eV, respectively. A comparison with XPS spectra of the reference compounds suggests that two different types of cobalt species were present on the calcined Co/Nb_2O_5 catalysts: Co_3O_4 particles and Co^{2+} surface species. At high cobalt content, Co_3O_4 particles were the main species, whereas the fraction of Co^{2+} species linked to the support enhanced as the cobalt loading decreased. The model proposed was confirmed by fitting the Co 2p spectra of the Co/Nb_2O_5 catalysts to the Co 2p spectra of reference compounds: Co_3O_4 and a Co^{2+} species (CoO, Co niobate at 873 K or Co niobate at 1173 K). The cobalt niobate calcined at 873 K was chosen as better representing the Co^{2+} surface phase on the niobia supported cobalt catalysts. These results agreed with DRS analyses, which detected the presence of a higher amount of octahedral Co^{2+} on the catalysts with low cobalt content.

In comparison with XPS spectra of the reference compounds and Co/Nb_2O_5 catalysts of the literature, the XPS analyses suggested the presence of Co_3O_4 particles and a Co^{2+} surface phase on Co/Nb_2O_5 and $PdCo/Nb_2O_5$ catalysts. The XPS spectrum of the Co/Nb_2O_5 and $Pd_{35}Co_{65}/Nb_2O_5$ bimetallic catalyst presented a strong shake-up satellite peak around 786 eV and a spin−orbit coupling of 16 eV. On the other hand, the $Pd_{15}Co_{85}/Nb_2O_5$ catalyst showed a weak satellite peak and a spin−orbit splitting of 15 eV. Then, the catalysts with low cobalt content (Co/Nb_2O_5 and $Pd_{35}Co_{65}/Nb_2O_5$) presented mainly Co^{2+} species, whereas Co_3O_4 particles were also formed, in addition to Co^{2+} species at high cobalt loading ($Pd_{15}Co_{85}/Nb_2O_5$).

Reduction of the Precursor. The TPR profiles of niobia-supported catalysts are presented in Figure 2. The Pd/Nb_2O_5 catalyst presented an important hydrogen uptake at room temperature because of palladium oxide reduction, hydrogen adsorption, and hydride formation.[37,63,64] It also exhibited a desorption peak at 341 K, which is generally attributed to desorption of reversible hydrogen from the palladium surface and to the decomposition of palladium hydride during the reduction of palladium oxide.[37,63,64] The total hydrogen consumption corresponded to a complete reduction of PdO (Table 3). The hydrogen consumption above 473 K was previously observed[36,64,65] and was ascribed to a partial reduction of the support, the first step of the SMSI formation.

The $2\%Co/Nb_2O_5$ catalyst did not exhibit reduction at room temperature. The reduction profile showed a broad peak at 753

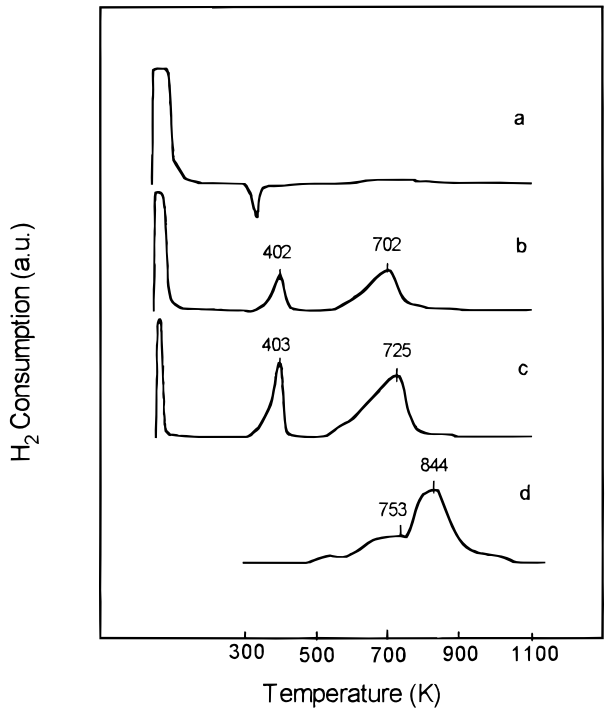

Figure 2. Reduction profiles of the niobia-supported catalysts. (a) Pd/Nb_2O_5; (b) $Pd_{35}Co_{65}/Nb_2O_5$; (c) $Pd_{15}Co_{85}/Nb_2O_5$; (d) Co/Nb_2O_5.

K and a large one at 844 K, in agreement with the literature.[12,66] Recently, we have also studied the effect of cobalt loading on the properties of niobia-supported cobalt catalysts.[12] TPR analyses were performed on Co_3O_4 and Co/Nb_2O_5 catalysts containing 1, 2, 5, and 10 wt % Co. The $10\%Co/Nb_2O_5$ catalyst presented three reduction peaks. The two peaks at low temperatures appeared at the same region of the reduction of bulk Co_3O_4, which correspond to the reduction in two steps: $Co_3O_4 \rightarrow CoO \rightarrow Co$. The peak at high temperature was attributed to the reduction of Co^{2+} species, in interaction with the support. The decrease of cobalt loading led to a decrease of the first two peaks. Then, at high cobalt content, Co_3O_4 particles were the main species, whereas the percentage of Co^{2+} surface phase increased as the cobalt loading decreased. In view of these results, the hydrogen uptake at 753 K could be attributed to the reduction of Co_3O_4 particles, whereas the reduction peak at 844 K could correspond to the reduction of Co^{2+} species interacting with niobia.

The reduction profiles of the bimetallic Pd−Co catalysts were very different from the profiles of Pd and Co monometallic catalysts, suggesting the existence of some interaction between the metals.[67] The bimetallic catalysts showed peaks at room temperature and at 400 and 700 K. The hydrogen consumption at room temperature (Table 3) was higher than the theoretical value expected for complete reduction of PdO, indicating that another process may occur besides PdO reduction. Because PdO was reduced completely at room temperature, the peaks at 400 and 700 K can be ascribed to the reduction of cobalt oxides. However, these maxima were shifted toward lower temperatures, compared with the cobalt reduction of the monometallic Co/Nb_2O_5 catalyst, indicating that palladium catalyzes the cobalt oxide reduction.

Therefore, the palladium addition promoted not only the reduction of Co_3O_4 particles but also the reduction of the cobalt surface phase as it was reported by Hoff.[24] The magnetic measurements coupled with TPR analyses will allow us to quantify this promotional effect.

TABLE 4: Reduction Degree Calculated from Magnetic Measurements after Reduction at Different Temperatures

	metallic Co (%)		
catalyst	T_{room}	298−473 K	473−873 K
Pd/Nb_2O_5	[a]	[a]	[a]
$Pd_{35}Co_{65}/Nb_2O_5$	4	12	105
$Pd_{15}Co_{85}/Nb_2O_5$	[a]	4	105
Co/Nb_2O_5	[a]	[a]	43

[a] Presented only a diamagnetic signal.

Saturation of magnetization was determined from the magnetization curves for each sample reduced at increasing temperatures, and the degree of reduction of cobalt was calculated (Table 4).

The Pd/Nb_2O_5 catalyst showed only a diamagnetic signal. The Co/Nb_2O_5 catalyst was not completely reduced at 873 K. The degree of reduction revealed only 43% cobalt in the metallic state, which was much lower than that calculated from the hydrogen uptake during the TPR. As discussed for the Pd/Nb_2O_5 catalyst, this difference could be attributed to a partial reduction of niobia at high temperatures.

The magnetic measurements of the $Pd_{35}Co_{65}/Nb_2O_5$ bimetallic catalyst showed the presence of 4% metallic cobalt even after reduction at room temperature, confirming the strong promoting effect of Pd on cobalt oxide reduction. After reduction at 473 K, the magnetic measurements indicated that 12% of cobalt was already in the metallic state (Table 4). However, the hydrogen consumption measured by TPR (Table 3) was higher than the amount of metallic cobalt produced, suggesting a partial transformation of Co_3O_4 to CoO in this temperature range as well. The reduction at 873 K led to a complete reduction of cobalt oxides, in opposition to the behavior observed on the Co/Nb_2O_5 catalyst. This result indicated that palladium also promoted the reduction of the Co^{2+} species, because XPS and TPR analysis revealed the presence of a cobalt surface phase. Thus, the magnetic measurements performed at different reduction temperatures support the TPR results, giving further evidence of the interaction between both metals.

In the $Pd_{15}Co_{85}/Nb_2O_5$ bimetallic catalyst reduced at room temperature, the magnetic measurements did not suggest the presence of metallic cobalt. After reduction at 473 K, the amount of metallic cobalt was lower than on $Pd_{35}Co_{65}/Nb_2O_5$ catalyst. In other words, the promoting effect of palladium decreases with the increase of cobalt loading. However, after reduction at 873 K, all cobalt oxide was reduced to a metallic state, as observed for the $Pd_{35}Co_{65}/Nb_2O_5$ catalyst.

A Model for the Bimetallic Catalysts. Several models for supported cobalt-noble metal have been reported[22,24,58,68] to explain the promoting effect of the noble metal on cobalt oxide reduction.

The TPR profiles of supported Rh−Co catalysts[22,68] showed that the reduction took place at lower temperatures than the monometallic Co catalyst. Van't Blik and Prins[22] suggested that the calcination led to the formation of two metal oxide phases (Rh_2O_3 and Co_3O_4), which are in close contact, and to the formation of the $CoAl_2O_4$ phase. During the reduction, bimetallic Co−Rh particles with a surface enrichment of cobalt were observed. EXAFS experiments exhibited clear evidence of Rh−Co alloy formation on $Rh-Co/SiO_2$ catalysts.[68]

On $Pt-Co/Al_2O_3$ catalysts, Zsoldos et al.[19] and Zsoldos and Guczi[58] proposed the presence of Co_3O_4 particles (easily reducible), a surface spinel and a Co surface phase containing Co^{3+} and Co^{2+} ions in octahedral lattice sites (nonreducible and partially reducible, respectively). At low cobalt content, $CoPt_3$ bimetallic particles were also observed after reduction.

According to Hoff,[24] the addition of Pt, Pd, Ir, and Ru to Co/Al_2O_3 catalyst promoted the reduction not only of the Co_3O_4 particles but also of the cobalt surface phase. The promotional effect of noble metals on the reduction of Co^{3+}/Co^{2+} surface layer was attributed to: (i) a dilution effect of the surface cobalt layer by the second metal, (ii) a physical coverage of the surface cobalt layer by the noble metal, or (iii) an oxidation of Co^{2+} to Co^{3+} during the calcination, due to the presence of the noble metal, as suggested by Sass et al.,[69] which decreases the extent of Co^{2+} diffusion into the alumina lattice.

Previous studies with graphite-supported Pd−Co catalysts[42,43] have shown that palladium promoted the reduction of cobalt oxides. The transmission electron microscopy results and local STEM analyses allowed the proposal of two mechanisms to explain the bimetallic formation: an intimate contact between both oxide particles and migration of the metal particles over the support because of graphite gasification phenomena. In this case, the participation of an H_2 spillover mechanism to explain the bimetallic formation was limited.

However, the description of niobia-supported bimetallic catalysts is still scarce. Recently,[60] XPS analysis of Rh−Co/Nb_2O_5 catalysts showed also the presence of two Co species at the surface: Co_3O_4 particles and Co^{2+} species. From XPS intensities, it was found that the Co_3O_4 particles formed thick islands, which were covered by Rh_2O_3 particles besides a surface phase of Co^{2+} oxide on Nb_2O_5.

In this work, XPS and TPR results revealed the presence of Co_3O_4 particles and a cobalt surface phase covering the niobia support. The palladium addition promoted the reduction of both Co_3O_4 particles and the cobalt surface species as revealed by TPR and magnetic measurements. These results are very consistent with those reported for cobalt-noble metal supported on alumina. Therefore, the following model could describe the niobia-supported Pd−Co catalysts, PdO and Co_3O_4 particles covering the cobalt surface layer or diluted by it. An intimate contact between PdO and cobalt oxide phases could explain the promoting effect of palladium on the cobalt oxides reduction.

Alloy Formation. Cobalt and palladium systems form a continuous series of solid solution and even-ordered phases (Pd_3Co and Pd−Co) can be observed in bulk alloys.[70−73]

Up to now, no precise information about the alloy formation was obtained on the Pd−Co/Nb_2O_5 catalysts. The magnetic measurement is a valuable tool to present direct evidence for the formation of a solid solution.[74,75]

Figure 3 shows the specific saturation magnetization of completely reduced catalysts. The values of bulk alloys were also presented for comparison (black line).[70]

After reduction at 773 K, the magnetic moment calculated for $Pd_{35}Co_{65}/Nb_2O_5$ catalyst was in good agreement with the corresponding values of bulk alloys, suggesting that supported Pd−Co alloys were obtained. On the other hand, in the $Pd_{15}Co_{85}/Nb_2O_5$ catalyst, the magnetic moment value was slightly lower than the one expected, suggesting the formation of a palladium-rich alloy (78 at. % of Co).

Recently, magnetic measurements on graphite-supported palladium−cobalt catalysts also revealed the formation of supported Pd−Co alloys in agreement with X-ray diffraction and EXAFS analyses.[42]

Bozorth et al.[70] showed that diluted solutions of cobalt on palladium are ferromagnetic and that the moment associated to one cobalt atom increased with the dilution. According to them, the Co moment induces a moment on the surrounding Pd atoms via electron polarization, thereby producing a greater overall moment. For the $Pd_{35}Co_{65}/Nb_2O_5$ catalyst the calculated magnetic moment was 2 μB per Co atom, whereas on the Co/Nb_2O_5 catalyst it was 1.7 μB. Our results thoroughly agree with this interpretation.

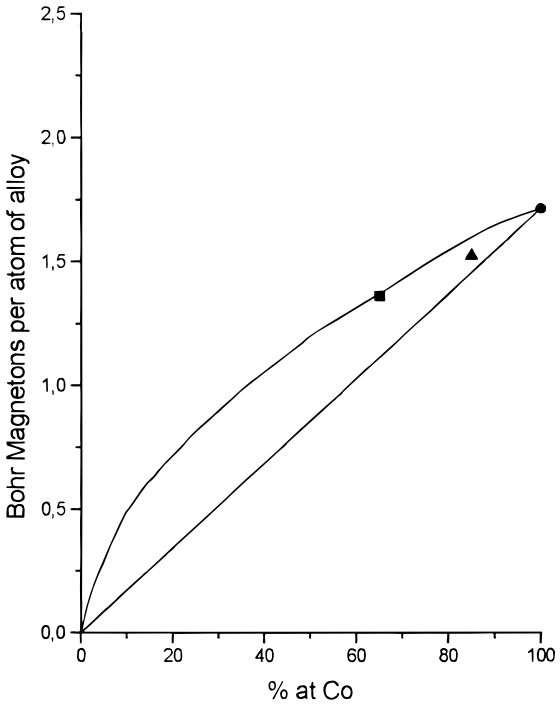

Figure 3. Ferromagnetic moments per atom of alloy of niobia-supported catalysts (points) and bulk alloys (line).[70]

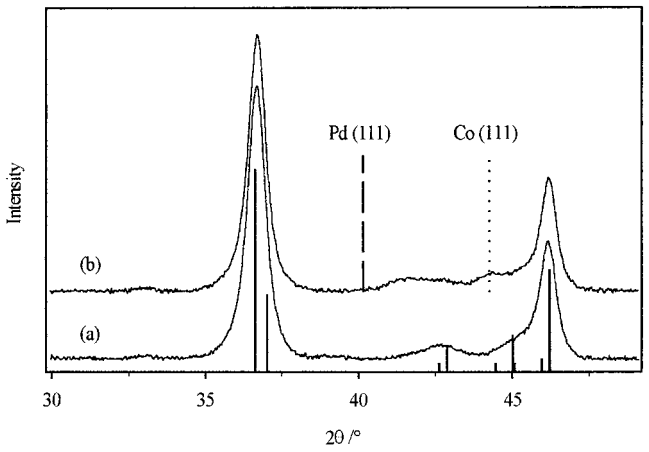

Figure 4. X-ray diffraction patterns of the $Pd_{15}Co_{85}/Nb_2O_5$ catalyst after reduction at 298 K (a) and 773 K (b). Vertical bars indicate the position of the Bragg peaks for Pd (−−) (JCPDS 46-1043); Co (·····) (JCPDS 15-0806); Nb_2O_5 (—) (JCPDS 30-0873).

This phenomenon of dilution of the magnetic moment in a nonmagnetic host (Pd), producing a total moment greater than that due to the solute alone, is called *giant moment* and confirms the presence of a Pd−Co alloy.[76]

X-ray diffraction analysis was performed only with the $Pd_{15}Co_{85}/Nb_2O_5$ catalyst, because only the lines characteristic of the support were observed on the bimetallic catalyst with lower cobalt content. After reduction at 773 K, the diagram exhibited a broad peak of $2\theta = 41°$, indicating the presence of a Pd-rich alloy (Figure 4). However, a peak characteristic of pure Co (111) was also observed. This means that isolated metallic cobalt particles were present together with the bimetallic phase.

XRD measurements also revealed the formation of a heterogeneous alloy on Pd−Co/carbon[77] and Pd−Co/graphite[42] cata-

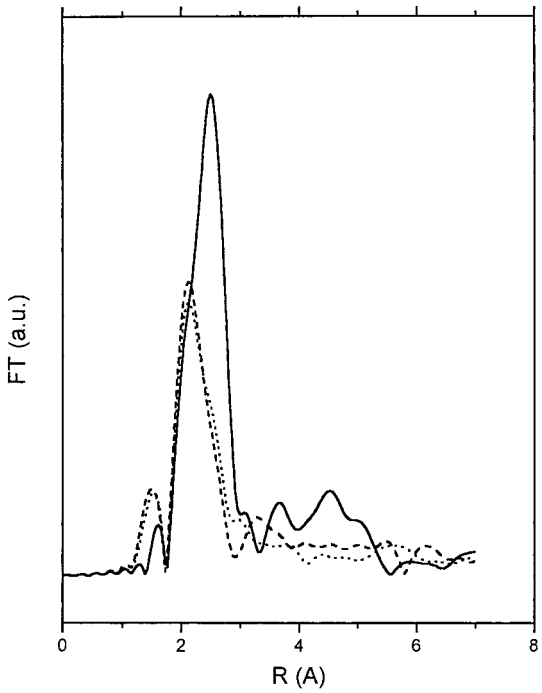

Figure 5. Amplitude of the radial distribution function at the Pd K edge for Pd foil (solid line), $Pd_{35}Co_{65}/Nb_2O_5$ (dashed line), $Pd_{15}Co_{85}/Nb_2O_5$ (dotted line).

lysts. According to Mallát et al.,[77] Pd−Co bimetallic catalysts presented Co or Co-rich disordered alloys in addition to a Pd-rich phase. In graphite-supported Pd−Co catalysts, the EDX analysis showed that all particles always contained palladium and cobalt with different compositions and particle size.[43]

On niobia-supported Pd−Co catalysts, the presence of isolated cobalt particles probably could be associated with the reduction of Co^{2+} species, initially linked to niobia. Despite the promoting effect of palladium reduction during TPR, these species remained alone after reduction because of a rather strong interaction with the carrier. The observation of a Pd-rich alloy by X-ray was in good agreement with the magnetic measurements.

The information obtained by XRD analysis, however, is limited to the catalysts containing high cobalt content. Thus, EXAFS technique was used to obtain both further evidence of Pd−Co interaction and the mean composition of bimetallic particles, mainly on the bimetallic catalyst with low cobalt loading.

Figure 5 displays the k^3 Fourier Transform (FT) of the EXAFS functions at the Pd K edge of the reference Pd foil and both $Pd-Co/Nb_2O_5$ bimetallic catalysts reduced at 773 K. The radial distribution functions (RDF) were not corrected for phase shifts so that the observed peaks are shifted to lower R values from the true interatomic distances. The RDF of bimetallic catalysts are different from the RDF values of reference sample, which suggests that the first coordination shell contains not only palladium atoms but also cobalt atoms in the niobia-supported Pd−Co catalysts.

The results of the fits obtained at the Pd K edge are summarized in Table 5. The curve fitting performed with both Pd and Co atoms in the first coordination sphere of Pd led to a decrease of the Q value, as seen in Figure 6 for $Pd_{15}Co_{85}/Nb_2O_5$. Moreover, the addition of Co atoms around palladium increased the total coordination number indicating the presence of large bimetallic particles. Furthermore, in the bimetallic catalysts the Pd−Pd distances obtained from the fit were close to those deduced from X-ray diffraction measurements on bulk alloys.[70] On the other hand, the value of the Pd−Co distance was in very good agreement with that obtained from the sum of the atomic radii of both elements (1.25 + 1.38 = 2.63 Å). The local atomic concentration of palladium, obtained by the $n_1/n_1 + n_2$ ratio,[40] was 64 and 87% on the $Pd_{35}Co_{65}/Nb_2O_5$ and $Pd_{15}Co_{85}/Nb_2O_5$ catalysts, respectively, indicating that the first shell around Pd atoms was clearly palladium enriched, which agreed well with magnetism and XRD analysis.

TABLE 5: EXAFS Results at the Pd K Edge of the Reference (Pd Foil) and Bimetallic Pd−Co Catalysts

	Pd−Pd			Pd−Co			
catalyst	n_1	R (Å)	$\Delta\sigma^2$ (Å^2)	n_2	R (Å)	$\Delta\sigma^2$ (Å^2)	Q (%)
Pd foil	12	2.75	0.000	−	−	−	−
$Pd_{35}Co_{65}$	5.77	2.66	0.000	−	−	−	14.4
6.29	2.67	0.000	3.59	2.62	0.0069	6.0	
$Pd_{15}Co_{85}$	5.91	2.65	0.000	−	−	−	16.9
7.93	2.67	0.000	1.40	2.63	0.0084	9.1	

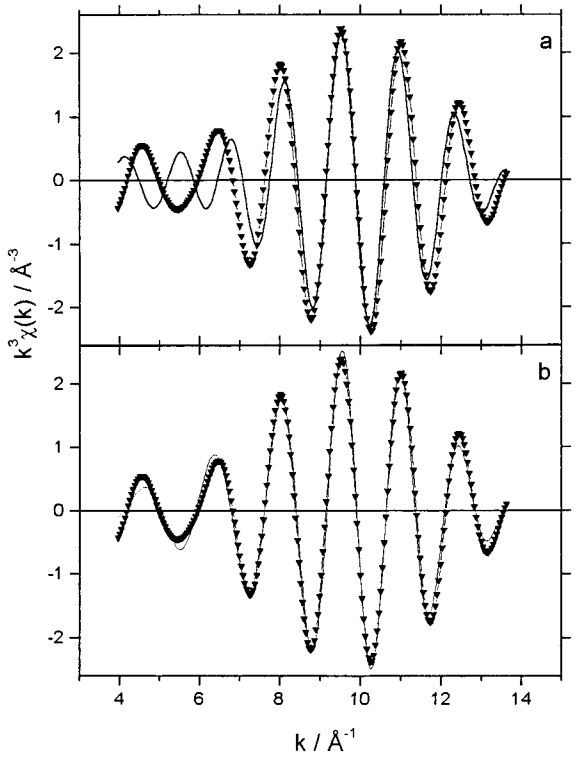

Figure 6. Inverse Fourier transform of the first peak at the Pd K edge for the $Pd_{15}Co_{85}/Nb_2O_5$ (solid line) and experimental points (triangles). (a) Curve fitting performed with Pd atoms in the first coordination sphere; (b) curve fitting performed with Pd and Co atoms in the first coordination sphere.

In Figure 7 we compare the Co K edge X-ray absorption near-edge (XANES) spectra of the bimetallic catalysts together with those of CoO, Co_3O_4, Co metal, and a $Pt_{25}-Co_{75}$ disordered single crystal. From the comparison of the spectra of the catalysts and the cobalt oxides it appears that cobalt is fully reduced as already deduced from magnetic measurements. But, more importantly, the similarity of shape between the spectra of the catalysts and of the disordered based platinum single crystal indicates that a large part of Co interacts with palladium. Moreover, because the shape of the XANES spectrum reflects the degree of filling of the Co valency band,[78] we may conclude that an electron transfer from Co to Pd took place, which may be important to explain the catalytic properties of Pd-based catalysts.

Figure 8 shows the RDF resulting from Fourier transformation of the EXAFS function at the Co K edge for the cobalt foil and

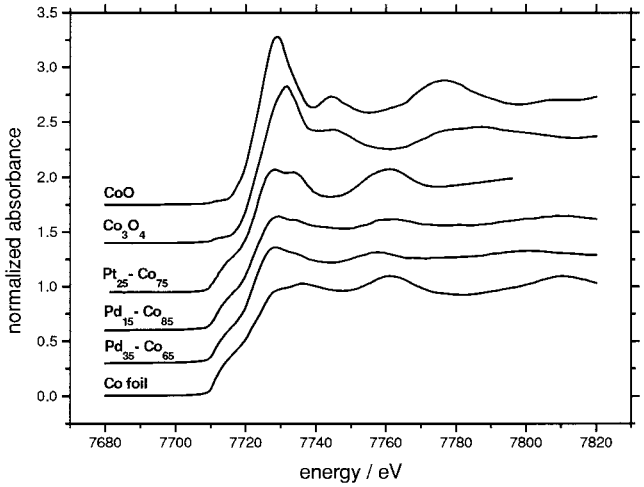

Figure 7. XANES spectra of cobalt oxides, $Pt_{75}Co_{25}$ disordered single crystal, $PdCo/Nb_2O_5$ catalysts, and Co foil (from top to bottom).

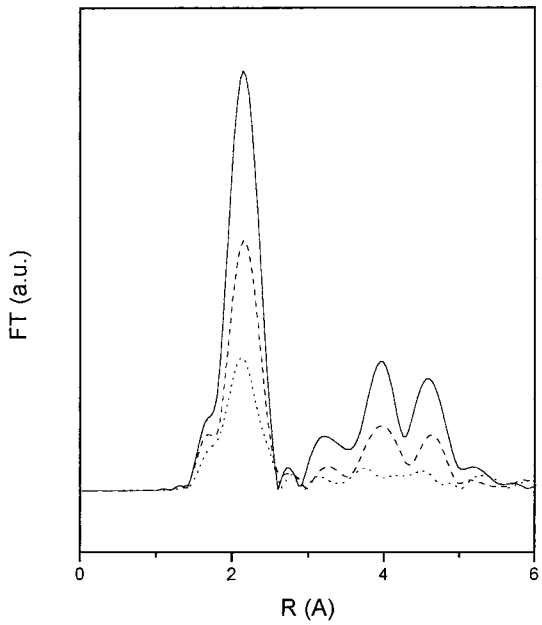

Figure 8. Amplitude of the radial distribution function at the Co K edge for Co foil (solid line), $Pd_{35}Co_{65}/Nb_2O_5$ (dashed line), $Pd_{15}Co_{85}/Nb_2O_5$ (dotted line).

TABLE 6: EXAFS Results at the Co K Edge of the Reference (Co Foil) and Bimetallic Pd−Co Catalysts

	Co−Co			Co−Pd			
catalyst	n_1	R (Å)	$\Delta\sigma^2$ (Å^2)	n_2	R (Å)	$\Delta\sigma^2$ (Å^2)	Q (%)
Co foil	12	2.51	0.000	–	–	–	–
$Pd_{35}Co_{65}$	3.58	2.49	0.000	–	–	–	23.9
	5.11	2.54	0.003	1.54	2.63	0.0050	6.97
$Pd_{15}Co_{85}$	6.94	2.51	0.000	–	–	–	14.1
	6.54	2.52	0.000	0.39	2.63	0.0021	9.25

the bimetallic catalysts. The structural parameters obtained by modeling of the first coordination sphere at the Co K edge are listed in Table 6, and the results of the fitting process are illustrated in Figure 9. The qualitative conclusion concerning the existence of a palladium−cobalt interaction obtained from Figure 7 was confirmed, and from these results it becomes evident that only a part of Co forms an alloy with palladium.

Therefore, the EXAFS analysis revealed the Pd−Co alloy formation during reduction, even on the bimetallic catalyst with low cobalt content. As observed through magnetism and XRD analysis, EXAFS results also suggested the presence of bimetallic particles enriched with palladium and particles containing only cobalt.

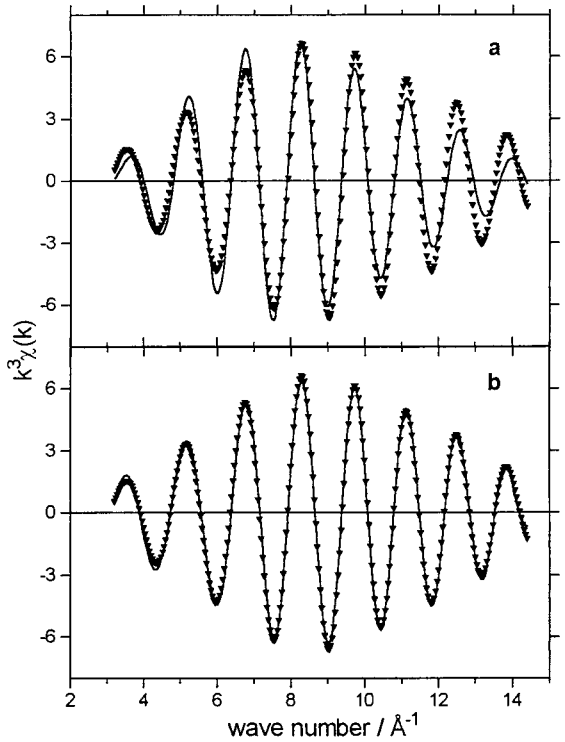

Figure 9. Inverse Fourier transform of the first peak at the Co K edge for the $Pd_{15}Co_{85}/Nb_2O_5$ (solid line) and experimental points (triangles). (a) Curve fitting performed with Co atoms in the first coordination sphere; (b) curve fitting performed with Pd and Co atoms in the first coordination sphere.

Based on the similarities with the alumina-supported noble metal−cobalt systems, it is possible to understand the catalytic behavior of noble metal−Co/Nb_2O_5 catalysts on CO hydrogenation.[35] As proposed by Guczi et al.[18] for $Pt-Co/Al_2O_3$ catalyst, the bimetallic particles could be responsible for the changes observed in selectivity. In our catalysts, these new sites were available for chain growth, as found through the enhancement of the C_5^+ selectivity,[35] but the selectivity for C_5^+ formation was improved after reduction at 773 K. Thus, the influence of the partially reduced NbO_x species on the mechanism cannot be discarded, as suggested by Silva et al.[66] for Co/Nb_2O_5 catalysts.

Conclusions

A surface model was proposed to represent the calcined Pd−Co/Nb_2O_5 catalysts where PdO and Co_3O_4 particles were covering a cobalt surface layer or diluted by it. The palladium addition promoted the reduction of the Co_3O_4 particles as well as the cobalt surface phase. After reduction at 773 K, a palladium-rich alloy was obtained. The presence of isolated metallic cobalt particles was probably associated with the reduction of Co^{2+} species, which remained alone in function of a strong interaction with the support.

Acknowledgment. We thank G. Bergeret for X-ray diffraction analysis and LURE for dedicated runs. F.B. Noronha also acknowledges CNPq for financial support.

References and Notes

(1) Anderson, R. B. *The Fischer−Tropsch Synthesis*; Academic Press Inc.; Orlando, 1984.

(2) Dry, M. E. In *Catalysis Science and Technology*; Anderson, J. R., Boudart, M., Eds.; Springer Verlog: Berlin, 1981; p 159.
(3) Holmen, A.; Jeus, K. J.; Kolboe, S. *Stud. Surf. Sci. Catal*. **1990**, 61.
(4) Reuel, R. C.; Bartholomew, C. H. *J. Catal*. **1984**, *85*, 78.
(5) Fu, L.; Bartholomew, C. H. *J. Catal*. **1985**, *92*, 376.
(6) Lee, J. H.; Lee, D. K.; Ihm, S. K. *J. Catal*. **1988**, *113*, 544.
(7) Ho, S. W.; Houalla, M.; Hercules, D. M. *J. Phys. Chem*. **1990**, *94*, 6396.
(8) Castner, D. G.; Santilli, D. S. *Catalytic Materials: Relationship between Structure and Reactivity*; Whyte, T. E., Dalla Beta, R. A., Derouane, E. G., Baker, R. T. K., Eds.; ACS Symposium Series 248; American Chemical Society: Washington, DC, 1984; p 39.
(9) Lapidus, A.; Krylova, A.; Kazanski, V.; Borovkov, V.; Zaitsev, A.; Rathousky, J.; Zukal, A.; Jancalkova, M. *Appl. Catal*. **1991**, *73*, 65.
(10) Arnoldy, P.; Moulijn, J. A. *J. Catal*. **1985**, *93*, 38.
(11) Sato, K.; Ionoue, Y.; Kojima, I.; Miyazaki, E.; Yasumori, I. *J. Chem.Soc., Faraday Trans*. **1984**, *80*, 841.
(12) Noronha, F. B.; Perez, C. A.; Frety, R.; Schmal, M. *Phys. Chem. Chem. Phys*. **1999**, *1*, 2861.
(13) Ho, S.; Cruz, J. M.; Houalla, M.; Hercules, D. *J. Catal*. **1992**, *135*, 173.
(14) Chin, R. L.; Hercules, D. M. *J., Phys., Chem*. **1982**, *86*, 360.
(15) Tung, H.; Yeh, C.; Hong, C. *J. Catal*. **1990**, *122*, 211.
(16) Stranick, M. A.; Houalla, M.; Hercules, D. M. *J. Catal*. **1987**, *103*, 151.
(17) Niemantsverdriet, J. W.; Louwers, S. P. A.; van Grondelle, J.; van der Kraan, A. M.; Kampers, F. W. H.; Konigsberger, D. C. *Proceedings of the Ninth International Congress on Catalysis*; Phillips, M. J., Ternan, M., Eds.; Chemical Institute: Ottawa, 1988; Vol. II, p 674.
(18) Guczi, L.; Hoffer, T.; Zoldos, Z.; Zyad, S.; Maire, G.; Garin, F. *J. Phys. Chem*. **1991**, *95*, 802.
(19) Zsoldos, Z.; Hoffer, T.; Guczi, L. *J. Phys. Chem*. **1991**, *95*, 798.
(20) Kapoor, M. P.; Lapidus, A. L.; Krylova, A. Y. *Proceedings of the Tenth International Congress on Catalysis*; Guczi, L., Solymosi, F., Tetenyi, P., Eds.; Elsevier: Budapest, 1992; Part C, p 2741.
(21) Schanke, D.; Vada, S.; Blekkan, E. A.; Hilmen, A. M.; Hoff, A.; Holmen, A. *J. Catal*. **1995**, *156*, 85.
(22) van't Blik, H. F. L.; Prins, R. *J. Catal*. **1986**, *97*, 188.
(23) Martens, J. H. A.; van't Blik, H. F. L.; Prins, R. *J. Catal*. **1986**, *97*, 200.
(24) Hoff, A., Dr. Ing. Thesis, Norges Tekniske Hogskole, 1993.
(25) Sarkany, A.; Zsoldos, Z.; Stefler, G.; Hightower, J. W.; Guczi, L. *J. Catal*. **1995**, *157*, 179.
(26) Idriss, H.; Diagne, C.; Hindermann, J. P.; Kinnemann, A.; Barteau, M. A. *Proceedings of the Tenth International Congress on Catalysis*; Guczi, L., Solymosi, F., Tetenyi, P., Eds.; Elsevier: Budapest, 1992; Part C, p 2119.
(27) Juszczyk, W.; Karpinski, Z.; Lomot, D.; Prelaszek, J.; Paál, Z.; Stakheev, A. Y. *J. Catal*. **1993**, *142*, 617.
(28) Ponec, V. *Catal. Rev. Sci. Eng*. **1975**, *11*, 41.
(29) Sachtler, W. M. H.; van Santen, R. A. *Adv. Catal*. **1977**, *26*, 69.
(30) Lietz, G.; Nimz, M.; Volter, J.; Lázár, K.; Guczi, L. *Appl. Catal*. **1988**, *45*, 71.
(31) Guczi, L. *Catal. Lett.* **1990**, *4*, 205.
(32) Woo, H. S.; Fleisch, T. H.; Foley, H. C.; Uchiyama, S.; Delgass, W. N. *Catal. Lett.* **1990**, *4*, 93.
(33) Fukushima, T.; Araki, K.; Ichikawa, M. *J. Chem. Soc*. **1986**, 148.
(34) Iglesia, E.; Soled, S. L.; Fiato, R. A.; Via, G. H. *J. Catal*. **1993**, *143*, 345.
(35) Noronha, F. B.; Frydman, A.; Aranda, D. A. G.; Perez, C. A.; Soares, R. R.; Moraweck, B.; Castner, D.; Campbell, C. T.; Frety, R.; Schmal, M. *Catal. Today* **1996**, *28*, 147.
(36) Noronha, F. B.; Primet, M.; Frety, R.; Schmal, M. *Appl. Catal*. **1991**, *78*, 125.
(37) Aranda, D. A. G.; Noronha, F. B.; Passos, F. B.; Schmal, M. *Appl. Catal. A* **1993**, *100*, 77.
(38) Pereira, M. M.;, Noronha, F. B.; Schmal, M. *Catal. Today* **1993**, *16*, 407.
(39) Dees, M. J.; Ponec, V. *J. Catal*. **1989**, *119*, 376.
(40) Faudon, J. F.; Senocq, F.; Bergeret, G.; Moraweck, B.; Clugnet, G.; Nicot, C.; Renouprez, A. *J. Catal*. **1993**, *144*, 460.
(41) Soma-Noto, Y.; Sachtler, W. M. H. *J. Catal*. **1974**, *32*, 315.
(42) Noronha, F. B.; Schmal, M.; Bergeret, G.; Moraweck, B.; Frety, R. *J. Catal.* **1999**, *186*, 20.
(43) Noronha, F. B.; Nicot, C.; Schmal, M.; Frety, R.; Moraweck, B. *J. Catal*. **1997**, *168*, 42.
(44) Moulder, J. F.; Stickle, W. F.; Sobol, P. E.; Bomben, K. D. In *Handbook of X-ray Photoelectron Spectroscopy*; Chaspain, J., Ed.; Perkin-Elmer Corp.: 1992.
(45) Scofield, J. H. *J. Electron Spectrosc. Relat. Phenom*. **1976**, *8*, 129.
(46) Seah, M. P.; Dench, W. A. *Surf. Interface Anal*. **1979**, *1*, 2.
(47) Dalmon, J. A. In *Les Techniques Physiques d'étude des Catalyseurs*; Imelik, B., Vendrine, J. C., Eds.; Editions Technip: Paris, 1988; p 791.
(48) Dalmon, J. A. *J. Catal*. **1979**, *60*, 325.
(49) Moraweck, B.; Renouprez, A. J. *Surf. Sci*. **1981**, *106*, 35.
(50) Lengeler, B.; Eisenberger, P. *Phys. Rev*. **1980**, *B21*, 4507.
(51) Nelder, J. A.; Mead, R. *Comput. J*. **1965**, *7*, 308.
(52) Rehr, J. J. *Physica* **1989**, *B158*, 1.
(53) Zsoldos, Z.; Sarkany, A.; Guczi, L. *J. Catal*. **1994**, *145*, 235.
(54) Otto, L.; Haack, L. P.; de Vries, J. E. *Appl. Catal*. **1991**, *B1*, 1.
(55) Castner, D. G.; Watson, P. R.; Chan, I. Y. *J. Phys.Chem*. **1989**, *93*, 3188.
(56) Moyes, R. B.; Roberts, M. W. *J. Catal*. **1977**, *49*, 216.
(57) Chung, K. S.; Massoth, F. E. *J. Catal*. **1980**, *64*, 320.
(58) Zsoldos, Z.; Guczi, L. *J. Phys. Chem*. **1992**, *96*, 9393.
(59) Okamoto, Y.; Imanaka, T.; Teranishi, S. *J. Catal*. **1980**, *65*, 448.
(60) Frydman, A.; Castner, D. G.; Schmal, M.; Campbell, C. T. *J. Catal*. **1995**, *152*, 164.
(61) McIntyre, N. S.; Cook, M. G. *Anal. Chem*. **1975**, *47*, 2210.
(62) Barr, T. L. *J. Phys. Chem*. **1978**, *82*, 1801.
(63) Chen, G.; Chou, W. T.; Yeh, C. T. *Appl. Catal*. **1983**, *8*, 389.
(64) Chang, T. C.; Chen, J. J.; Yeh, C. T. *J. Catal*. **1985**, *96*, 51.
(65) Hu, Z.; Kunimori, K.; Uchijima, T. *Appl. Catal*. **1991**, *69*, 253.
(66) Silva, R. R. M.; Dalmon, J. A.; Frety, R.; Schmal, M. *J. Chem. Soc. Faraday Trans*. **1993**, *89*, 3975.
(67) Anderson, J. R.; Pratt, K. C. In *Introduction to Characterization and Testing of Catalysts*; Academic Press: Sidney, 1985.
(68) van't Blik, H. F. L.; Koningsberger, D. C.; Prins, R. *J. Catal*. **1986**, *97*, 210.
(69) Sass, A. S.; Shvets, V. A.; Savel'eva, G. A.; Kazanskii, V. B. *Kinet. Katal*. **1985**, *26*, 1149.
(70) Bozorth, R. M., Wolff, P. A., Davis, D. D.; Compton, V. B.; Wernick, J. M. *Phys. Rev*. **1961**, *B122*, 1157.
(71) Matsuo, Y. *J. Phys. Soc. Jpn*. **1972**, *32*, 972.
(72) Mallát, T.; Petró, J.; Szabó, S.; Marczis, L. *J. Electroanal. Chem*. **1986**, *208*, 169.
(73) Mallát, T.; Szabó, S.; Petró, J. *Acta Chim. Hung*. **1987**, *124*, 47.
(74) Raab, C.; Lercher, J. A.; Goodwin, J. G.; Shyu, J. *J. Catal*. **1990**, *122*, 406.
(75) Sinfelt, J. H.; Carter, J. L.; Yates, D. J. C. *J. Catal*. **1972**, *24*, 283.
(76) Mydosch, J. A.; Nieuwenhuys, G. J. In *Ferromagnetic Materials. A Handbook on the Properties of Magnetically Ordered Substances*; Wolfarth, E. P., Ed.; North-Holland Publishing Company: Amsterdam, 1980; Vol. 1.
(77) Mallat, T.; Szabo, S.; Petro, J.; Mendioroz, S.; Folgado, M. A. *Appl. Catal*. **1989**, *53*, 29.
(78) Hlil, E. K.; Baudoing-Savois, R.; Moraweck, B.; Renouprez, A. J. *J. Phys. Chem*. **1996**, *100*, 3102.